

1 **Autophagy Suppresses CCL2 to Preserve Appetite and Prevent Lethal Cachexia**

2

3 Maria Ibrahim^{1,2}, Maria Gomez-Jenkins^{1,2}, Adina Scheinfeld², Zhengqiao Zhao³ Eduardo Cararo
4 Lopes¹, Akshada Sawant^{1,2}, Zhixian Hu^{1,2}, Aditya Dharani¹, Michael Sun¹, Sarah Siddiqui¹,
5 Emily T. Mirek⁴, Johan Abram-Saliba⁵, Edmund C. Lattime^{1,6} Xiaoyang Su^{1,6}, Tobias
6 Janowitz⁷, Marcus D. Goncalves⁸, Steven M. Dunn⁵, Yuri Pritykin^{2,3,9}, Tracy G. Anthony^{1,2,4},
7 Joshua D. Rabinowitz², Eileen White^{1,2*}

8 1. Rutgers Cancer Institute, Rutgers University, New Brunswick, NJ 08903, USA

9 2. Ludwig Princeton Branch, Ludwig Institute for Cancer Research, Princeton University,
10 Princeton, NJ 08544, USA

11 3. Lewis-Sigler Institute for Integrative Genomics, Princeton University, Princeton, NJ
12 08540, USA

13 4. Department of Nutritional Sciences, Rutgers School of Environmental and Biological
14 Sciences, Rutgers University, New Brunswick, NJ 08901, USA

15 5. LAbCore Immunoglobulin Discovery Platform, Department of Oncology, Ludwig
16 Institute for Cancer Research-Lausanne, University Hospital and University of Lausanne,
17 1066, Epalinges, Switzerland

18 6. Department of Medicine, Rutgers Robert Wood Johnson Medical School, New
19 Brunswick, NJ 08901, USA

20 7. Cold Spring Harbor Laboratory, Cold Spring Harbor, NY 11724, USA; Northwell Health
21 Cancer Institute, Northwell Health, New Hyde Park, NY 11042, USA

22 8. Departments of Medicine and Radiation Oncology, New York University, Grossman
23 School of Medicine, Laura and Isaac Perlmutter Cancer Center, New York, NY 10016,
24 USA

25 9. Department of Computer Science, Princeton University, Princeton, NJ 08540, USA

26 *Corresponding author:

27 Eileen White, epwhite@cinj.rutgers.edu

28

29 Key points of paper:

- 30 1) Autophagy-deficient mice have reduced food intake, systemic inflammation, and cachexia
- 31 2) CCL2, but not GDF15 or CXCL10, induces lethal cachexia caused by autophagy defect
- 32 3) Autophagy-deficient mice have CCL2-dependent destruction of appetite-promoting neurons
33 in the hypothalamus
- 34 4) Leptin deficiency restores appetite and rescues lethal cachexia in autophagy-deficient mice
- 35 5) Autophagy-deficient mice die from cachexia mediated by appetite loss
- 36 6) Degenerative conditions due to impaired autophagy are caused by the inflammatory response
37 to the damage
- 38 7) Targeting CCL2 may be a viable approach to prevent degenerative wasting disorders

39 Abstract

40 Macroautophagy (autophagy hereafter) captures intracellular components and delivers them to
41 lysosomes for degradation and recycling¹. In adult mice, autophagy sustains metabolism to
42 prevent wasting by cachexia and to survive fasting, and also suppresses inflammation, liver
43 steatosis, neurodegeneration, and lethality^{2,3}. Defects in autophagy contribute to metabolic,
44 inflammatory and degenerative diseases, however, the specific mechanisms involved were
45 unclear⁴. Here we profiled metabolism and inflammation in adult mice with conditional, whole-
46 body deficiency in an essential autophagy gene and found that autophagy deficiency altered fuel
47 usage, and reduced ambulatory activity, energy expenditure, and food intake, and elevated
48 circulating GDF15, CXCL10, and CCL2. While deletion of *Gdf15* or *Cxcl10* provided no or mild
49 benefit, deletion of *Ccl2* restored food intake, suppressed cachexia and rescued lethality of
50 autophagy-deficient mice. To test if appetite suppression by CCL2 was responsible for lethal
51 cachexia we performed single nucleus RNA sequencing of the hypothalamus, the center of
52 appetite control in the brain. Notably, we found that autophagy deficiency was specifically toxic
53 to PMCH and HCRT neurons that produce orexigenic neuropeptides that promote food intake,
54 which was rescued by deficiency in CCL2. Finally, the restoration of food intake via leptin
55 deficiency prevented lethal cachexia in autophagy-deficient mice. Our findings demonstrate a
56 novel mechanism where autophagy prevents induction of a cachexia factor, CCL2, which
57 damages neurons that maintain appetite, the destruction of which may be central to degenerative
58 wasting conditions.

59

60 Main

61 Autophagy is regulated by the autophagy-related genes (*Atg*) that function to assemble
62 autophagosomes and capture cargo including intracellular proteins and organelles, for degradation
63 and recycling. Macromolecules produced by autophagy recycling support metabolism and
64 eliminate damaged proteins and organelles thereby suppressing inflammation^{5,6}. Autophagy
65 recycling is essential for cell survival in mammals during the absence of nutrients. *Atg5*- or *Atg7*-
66 deficient mice are born developmentally normal but fail to survive the neonatal starvation period
67 due, in part, to nutrient insufficiency^{1,7}. Moreover, fasting is lethal to adult mice with conditional,
68 whole-body deletion of *Atg5* or *Atg7* due to hypoglycemia and wasting of muscle and adipose

69 tissue characteristic of cachexia^{2,3}. Thus, the evolutionary conserved function of autophagy is
70 sustaining metabolic homeostasis and survival to nutrient deprivation.

71

72 Autophagy is also important in the fed state, however, the specific mechanisms are unclear.
73 Conditional ablation of *Atg5* or *Atg7* in adult mice leads to liver inflammation and
74 neurodegeneration, and also weight loss, adipose tissue lipolysis and muscle atrophy, and body
75 wasting characteristic of cachexia^{2,3,8}. The lifespan of adult mice with conditional deficiency in
76 autophagy is limited to less than 3 months^{2,3}. Interestingly, neuronal-specific *Atg5* expression
77 rescues the neonatal lethality of *Atg5*-deficient mice⁷, however, the aspect of neuronal function
78 that is required to enable survival and if or how this is related to cachexia is unknown⁹. We found
79 that autophagy suppresses CCL2 thereby preserving hypothalamic neurons and food intake, which
80 prevents lethal cachexia. Thus, CCL2 is a cachexia factor responsible for hypothalamic neuron
81 degeneration leading to anorexia and death.

82

83 **Results**

84 **Autophagy deficiency leads to weight loss, altered body composition, liver inflammation,** 85 **and cachexia**

86 To investigate the role of autophagy in whole-body metabolism and cachexia, we analyzed body
87 composition in conditional whole-body *Atg7*-deficient (*Atg7^{Δ/Δ}*) compared to autophagy-intact
88 (*Atg7^{+/+}*) mice. At ten weeks post-deletion, *Atg7^{Δ/Δ}* mice showed consistent reduction in body
89 weight and a greater percent decrease from their initial body weight (Fig. 1a, S1a). *Atg7^{Δ/Δ}* mice
90 also exhibited reduced lean mass, progressive fat mass depletion (Fig. 1b-c) with lower weights
91 of white and brown adipose tissue, as well as soleus and gastrocnemius plantaris muscles,
92 compared to *Atg7^{+/+}* mice (S1b-c). Previous studies have shown that short-term
93 conditional *Atg7* deletion results in liver inflammation, steatosis, and hepatomegaly^{2,10,11}. At ten
94 weeks post-deletion, when liver weight was excluded from body weight, a further reduction in
95 weight was observed in *Atg7^{Δ/Δ}* mice (Fig. 1d). Thus, the reduction in body weight seen in
96 *Atg7^{Δ/Δ}* mice is an underestimate of body wasting due to the enlarged liver. In *Atg7^{Δ/Δ}* mice,
97 serum levels of liver enzymes alanine aminotransferase (ALT) and aspartate aminotransferase
98 (AST) were elevated, indicating liver inflammation and impaired function (Fig. S1d). To explore
99 the relationship between weight loss, systemic inflammation, and autophagy deficiency, we

100 performed RNA sequencing on livers from *Atg7^{Δ/Δ}* mice and compared them to *Atg7^{+/+}* controls
101 (Fig. S1e). GSTA1, GSTM1, and GSTM3 are genes encoding Glutathione S-Transferases
102 (GSTs), which play a key role in oxidative stress response and detoxification by conjugating
103 reduced glutathione to toxins, were significantly upregulated in the livers of *Atg7^{Δ/Δ}* mice.
104 Moreover, expression of two pro-inflammatory cytokines, CXCL10 and CCL2 were upregulated
105 in *Atg7^{Δ/Δ}* mice liver consistent with the known role of autophagy in suppressing damage and
106 inflammation in the liver^{2,12}.

107
108 To monitor metabolic activity in *Atg7^{Δ/Δ}* and *Atg7^{+/+}* mice they were assessed in metabolic cages
109 every two weeks post-deletion. Conditional whole-body *Atg7*-deficient mice and mice
110 lacking *Atg7* specifically in the central nervous system present with abnormal limb-clasping
111 reflexes and behavioral defects^{2,13,14}. Accordingly, we measured behavioral activity through
112 ambulatory activity and total wheel running and found *Atg7^{Δ/Δ}* mice displayed lower activity
113 compared to *Atg7^{+/+}* mice (Fig. e-f). Ambulatory activity analysis revealed a significant decrease
114 at each timepoint in *Atg7^{Δ/Δ}* mice (Fig. S1f). These findings are consistent with neurodegeneration
115 attributed to deficient autophagy¹⁵.

116
117 The respiratory exchange ratio (RER), which represents the ratio of produced CO₂ to consumed
118 O₂ is reflective of the major types of macronutrients being metabolized (lipids vs. carbohydrates).
119 Hourly RER plots at 2- and 8-weeks post-deletion revealed that *Atg7^{Δ/Δ}* mice exhibited higher RER
120 values compared to *Atg7^{+/+}* mice during the dark phase when mice are active (Fig. 1g). RER
121 analysis across both light and dark phases showed that this increase was statistically significant
122 during the dark phase at each time point (Fig. 1h, S1g). These findings suggest a shift away from
123 fat and/or toward carbohydrate (glucose) utilization as the preferred fuel source. This observation
124 aligns with previous studies showing glycogen depletion in the liver of adult mice with conditional
125 autophagy deficiency^{2,16} and may indicate a compensatory reliance on alternative nutrient sources
126 due to a metabolic deficit. In contrast, no differences were observed between *Atg7^{Δ/Δ}* and
127 *Atg7^{+/+}* mice during the light phase for RER when mice are inactive (Fig. 1h, S1g).

128
129 Involuntary weight loss is often linked to reduced appetite and/or increased energy expenditure,
130 which disrupts energy homeostasis. Total energy expenditure (TEE), which encompasses basal

131 metabolism, thermoregulation, physical activity, and the thermic effect of food intake, was reduced
132 in *Atg7^{Δ/Δ}* mice, failing to account for weight loss (Fig. 1i). Remarkably, we found that
133 *Atg7^{Δ/Δ}* mice exhibited significantly lower food intake compared to *Atg7^{+/+}* mice (Fig. 1j),
134 surprising given that they are intolerant to fasting, but possibly explaining loss of lean and fat
135 mass. As cytokines and chemokines can regulate appetite^{17,18} we measured these factors in the
136 serum (Fig. S1h). We found three factors that were significantly upregulated in the circulation of
137 *Atg7^{Δ/Δ}* mice compared to *Atg7^{+/+}* mice: Growth differentiation factor 15 (GDF15), C-X-C motif
138 chemokine ligand 10 (CXCL10), and C-C motif ligand 2 (CCL2) (Fig. 1k). Thus, autophagy-
139 deficient mice display a cachexia-like syndrome, including loss of body weight, appetite, and
140 wasting of muscle and fat, and increased levels of circulating cytokines and chemokines.

141

142 **CCL2 is the dominant factor responsible for lethal cachexia in autophagy-deficient mice**

143 To determine if GDF15, CXCL10 or CCL2 contribute to cachexia in autophagy-deficient mice,
144 we generated double knockout mice for each factor on the conditional *Atg7^{Δ/Δ}* background. GDF15
145 is a hormone known to reduce food intake^{19,20} by causing food aversion via signaling through
146 specific neurons in the area postrema and the nucleus of the solitary tract that express its receptor
147 GFRAL^{21,22}. To determine whether GDF15 modulates the lethality in autophagy deficiency, we
148 generated mice with constitutive deficiency in *Gdf15*^{23,24} and crossed them to *Ubc-Cre^{ERT2/+}*;
149 *Atg7^{flox/flox}* mice to generate *Gdf15^{-/-}*; *Ubc-Cre^{ERT2/+}*; *Atg7^{flox/flox}* mice. Tamoxifen (TAM)
150 administration was used to delete *Atg7* in the presence and absence of GDF15 (Fig. S1i). The loss
151 of GDF15, however, neither rescued the lethality caused by autophagy deficiency (Fig. S1i) nor
152 did it impact any other obvious phenotype.

153

154 CXCL10 is a chemokine induced in association with metabolic diseases²⁵ and infection²⁵⁻²⁷. To
155 investigate whether CXCL10 induction contributed to altered metabolism and reduced survival
156 caused by autophagy deficiency, mice with constitutive deficiency in *Cxcl10*²⁷ were crossed
157 with *Ubc-Cre^{ERT2/+}*; *Atg7^{flox/flox}* mice to generate *Cxcl10^{-/-}*; *Ubc-Cre^{ERT2/+}*; *Atg7^{flox/flox}* mice. TAM
158 administration was used to delete *Atg7* in the presence and absence of CXCL10 (Fig. S1j).
159 *Cxcl10^{-/-}*; *Atg7^{Δ/Δ}* mice demonstrated a small but significant improvement in survival compared to
160 *Atg7^{Δ/Δ}* mice, with median survival increased from 64 days to 134 days (Fig. S1j). These results
161 suggest that CXCL10 modestly extends survival, but neither GDF15 nor CXCL10 deficiency is

162 sufficient to substantially rescue weight loss, food intake, and lethality resulting from autophagy
163 deficiency.

164

165 CCL2 is a chemokine that recruits monocytes, macrophages, and other immune cells to sites of
166 injury or infection^{23,28}. It has been previously implicated in cancer-induced cachexia²⁹, specifically
167 metabolic changes in muscle and white adipose tissue (WAT)³⁰. To test whether CCL2 impacts the
168 survival of mice lacking autophagy, mice with constitutive deficiency in *Ccl2*²³ were crossed
169 with *Ubc-Cre*^{ERT2/+}; *Atg7*^{flox/flox} mice to generate *Ccl2*^{-/-}; *Ubc-Cre*^{ERT2/+}; *Atg7*^{flox/flox} mice. TAM
170 administration was used to delete *Atg7* in the presence and absence of CCL2 (Fig. 2Sa). While
171 *Atg7*^{Δ/Δ} mice survived less than three months², the loss of CCL2 completely rescued lethality
172 induced by autophagy deficiency (Fig. 2a). Notably, loss of CCL2 did not induce major alterations
173 in the cytokine and chemokine profile comparing *Atg7*^{Δ/Δ} and *Atg7*^{+/+} mice, suggesting that it may
174 function directly (Fig. S2b).

175

176 To determine how eliminating CCL2 rescued lethality of autophagy-deficient mice we
177 characterized the phenotypes of the four mouse genotypes. Histologic examination of tissues by
178 H&E showed that CCL2 deficiency mitigated tissue damage resulting from loss of autophagy
179 including liver inflammation, depletion of the lipid content of white adipose tissue (WAT) and
180 brown adipose tissue (BAT), and atrophy of skeletal muscle (Fig. S2c). Notably, the physical
181 appearance of cachexia, the increased livers weights, and the impaired liver function was
182 diminished in the *Ccl2*^{-/-}; *Atg7*^{Δ/Δ} compared to *Atg7*^{Δ/Δ} mice (Fig. 2b, Sd-e). While *Atg7*^{Δ/Δ} mice
183 develop evidence of severe hepatic dysfunction, as assessed by hyperbilirubinemia, low
184 triglyceride levels, and low blood urea nitrogen (BUN), the *Ccl2*^{-/-}; *Atg7*^{Δ/Δ} mice were protected
185 (Fig. S2f). Together, these results suggested that CCL2 plays a crucial role in maintaining survival
186 and preventing tissue damage upon loss of autophagy.

187

188 CCL2 induction is associated with weight loss including depleting muscle and adipose tissue while
189 also inducing liver steatosis²⁹, particularly during systemic inflammation³¹ and
190 neurodegeneration³² similar to what we observed in autophagy-deficient animals. As such,
191 therapeutic targeting of CCL2 with antibodies was attempted, but unfortunately without success³³.
192 To test if inhibiting CCL2 with an antibody was equivalent to genetic *Ccl2* deficiency we

193 regenerated the C1142 monoclonal antibody (mAb) proposed to neutralize circulating CCL2^{34,35}.
194 Following TAM-induced autophagy deficiency, mice were treated with either C1142 mAb or an
195 IgG control antibody. While *Atg7^{Δ/Δ}* mice treated with either C1142 mAb or IgG mAb showed no
196 difference in survival (Fig. S2g), the *Atg7^{Δ/Δ}* mice treated with C1142 mAb showed partial rescue
197 of body weight over time compared to IgG mAb (Fig. S2h). However, this result was due to an
198 increase in lean mass from further increased hepatomegaly in *Atg7^{Δ/Δ}* mice rather than a prevention
199 of adipose and skeletal muscle wasting (Fig. S2i). These data suggest that an antibody directed
200 against a CCL2 peptide does not phenocopy genetic deletion of *Ccl2*. Notably, CCL2 levels in the
201 liver of *Atg7^{Δ/Δ}* mice treated with C1142 mAb showed a decreasing trend compared to IgG-treated
202 mice, although no significant (Fig. S2j). These observations are in agreement with previous clinical
203 trial observations with therapeutic anti-CCL2 candidates that similarly failed to deplete the
204 chemokine³⁶. Moreover, they suggest that previous attempts to target CCL2 with an antibody in
205 vivo were likely ineffective and perhaps counterproductive.

206

207 **Loss of CCL2 rescues fasting lethality by preserving liver gluconeogenesis**

208 The loss of CCL2 extends lifespan and attenuates tissue damage in *Atg7^{Δ/Δ}* mice (Fig. 2a,S2c).
209 Therefore, we sought to investigate if elevated CCL2 levels also contributed to the fasting-induced
210 mortality due to hypoglycemia in autophagy-deficient mice^{2,3}. Mice were subjected to fasting (free
211 access to water without food for 24 hours). In contrast to the *Atg7^{Δ/Δ}* mice that die upon fasting,
212 *Ccl2^{-/-};Atg7^{Δ/Δ}* mice survive (Fig. 2c). Blood glucose and serum insulin levels during fasting were
213 maintained in *Ccl2^{-/-};Atg7^{Δ/Δ}* compared to *Atg7^{Δ/Δ}* mice, which present with hypoglycemia and
214 reduced insulin levels (Fig. 2d). We hypothesized that elevated blood glucose levels in
215 *Ccl2^{-/-};Atg7^{Δ/Δ}* compared to *Atg7^{Δ/Δ}* mice resulted from preservation of liver function and the
216 ability to perform gluconeogenesis during fasting. To test this hypothesis, we measured
217 gluconeogenesis by injecting mice with L-Lactate and then measuring the resulting glucose levels
218 in the blood. *Atg7^{Δ/Δ}* mice showed impaired ability to utilize lactate for glucose synthesis compared
219 to *Ccl2^{-/-};Atg7^{Δ/Δ}* mice, which maintained this capacity (Fig. 2e). To confirm that loss of CCL2
220 restored hepatic gluconeogenesis in autophagy-deficient mice, we performed *in vivo* ¹³C lactate
221 tracing. The labeled lactate in the plasma of *Atg7^{Δ/Δ}* mice was significantly higher as compared to
222 *Ccl2^{-/-};Atg7^{Δ/Δ}* mice (Fig. 2f), while the plasma glucose enrichment levels remained unchanged
223 between the groups (Fig. 2h). However, the ratio of glucose to lactate showed that significantly

224 less lactate was being converted to glucose in *Atg7^{Δ/Δ}* compared to *Ccl2^{-/-};Atg7^{Δ/Δ}* mice (Fig. 2i).
225 These findings demonstrated that *Atg7^{Δ/Δ}* mice are unable to efficiently utilize circulating lactate
226 for gluconeogenesis, resulting in reduced blood glucose levels and lethality upon fasting due to
227 hepatic dysfunction. In contrast, *Ccl2^{-/-};Atg7^{Δ/Δ}* mice effectively convert lactate to glucose via
228 gluconeogenesis, maintaining blood glucose levels and animal survival during fasting.

229

230 **CCL2 deficiency rescues weight and food intake but not fuel utilization or ambulatory** 231 **activity**

232 In contrast to *Atg7^{Δ/Δ}* mice, *Ccl2^{-/-};Atg7^{Δ/Δ}* mice maintained body weight, lean mass, and fat mass
233 (Fig. 3a-c) in addition to survival. Interestingly, *Ccl2^{-/-}* mice presented with a larger initial body
234 weight, gained significantly more weight compared to the other genotypes, and accumulate larger
235 lipid deposits in adipose tissues compared to *Atg7^{+/+}* mice (Fig. 3a-c, S2c). Together these results
236 suggest a role for CCL2 in regulating body composition.

237

238 Metabolic phenotyping found *Ccl2^{-/-};Atg7^{Δ/Δ}* and *Atg7^{Δ/Δ}* mice showed no significant difference
239 in the RER, suggesting nutrient utilization and preference was similar (Fig. 3e-f). Ambulatory
240 activity also showed no significant difference between *Ccl2^{-/-}Atg7^{Δ/Δ}* compared to *Atg7^{Δ/Δ}* mice
241 (Fig. 3d) and there was partial rescue in progressive motor, ataxia, and behavioral deficits in
242 *Ccl2^{-/-};Atg7^{Δ/Δ}* compared to *Atg7^{Δ/Δ}* mice (Fig. S2k) and Supplementary Movie S1. Brain
243 histological analyses showed the numbers of pyramidal neurons and Purkinje cells, related to
244 motor function and coordinated movement, were significantly increased in
245 *Ccl2^{-/-};Atg7^{Δ/Δ}* compared to *Atg7^{Δ/Δ}* mice (Fig. S2l). These results indicated that induction of
246 CCL2 in autophagy deficient mice was not responsible for alternated RER or defective ambulatory
247 activity although there was some preservation of Purkinje cells in the cerebellum and some
248 mitigation of defective hindlimb clasping. Eliminating CCL2, therefore, does not rescue all
249 autophagy-defect related phenotypes and would not be expected to correct cell damage induced
250 by failure of protein and organelle clearance critical to the function of post-mitotic and motor
251 neurons³⁷.

252

253 As shown above, *Atg7^{Δ/Δ}* mice have decreased food intake, TEE, and high levels of CCL2. We
254 therefore measured TEE and food intake in *Ccl2^{-/-}* and *CCL2^{-/-}; Atg7^{Δ/Δ}* mice. Loss of CCL2

255 restored TEE comparable to *Atg7^{+/+}* mice (Fig. 3g). Interestingly, *Ccl2^{-/-}* mice exhibited increased
256 food consumption during the dark and light cycle when compared to *Atg7^{+/+}* mice (Fig. 3h).
257 Surprisingly, loss of CCL2 significantly preserved food intake in *Ccl2^{-/-};Atg7^{Δ/Δ}* mice compared to
258 *Atg7^{Δ/Δ}* mice at both 2- and 8-weeks post deletion. (Fig. 3h). These results suggest that CCL2
259 induction in autophagy-deficient mice inhibited appetite, decreased food intake, and disrupted
260 energy homeostasis, which would be potentially lethal as they are intolerant to fasting.

261

262 **Eliminating CCL2 rescues loss of appetite-promoting hypothalamic neurons**

263 The ability of CCL2 deficiency to preserve food intake in autophagy-deficient mice suggested that
264 CCL2 may be toxic to neurons in the hypothalamus that express its cognate receptor, CCR2, and
265 produce hormones that regulate food intake³⁸. To test this hypothesis, single nucleus RNA
266 sequencing (snRNA-seq) was applied to the hypothalamus from wild-type and *Ccl2^{-/-}* mice with
267 and without deletion of *Atg7*. The hypothalami were pooled with four samples per genotype due
268 to the low weight of the tissue. This analysis yielded 20,297 high-quality single-nucleus
269 transcriptomes (Fig. 4a, S3a). Using molecular markers of known hypothalamic regions and cell
270 types³⁹, we were able to annotate the major hypothalamic cell type populations for each of the four
271 mouse genotypes (Fig. 4b). We identified 52 clusters that were classified into 28 broad cell types,
272 including astrocytes, fibroblast, oligodendrocytes, GABAergic (GABA) and glutamatergic (GLU)
273 neurons (Fig. 4b). UMAP embedding of each model is also shown (Fig. 4c, S3b). UMAP
274 embedding of each model is also shown (Fig. 4c, S3b). Notably, a cell subpopulation forming
275 Cluster 4 did not match to any known cell types from prior studies (Fig. 4a)³⁹. Cells in Cluster 4
276 had a higher level of mitochondrial gene expression and lower overall snRNA-seq signal than
277 other clusters, suggesting they were more likely apoptotic (Fig. S3c). Cluster 4 cells were
278 predominately from the *Atg7^{Δ/Δ}* hypothalamus (Fig. 4c,d), as compared with the remaining clusters
279 which had a relatively even distribution across the four genotypes. Note that CCL2 expression was
280 predominantly in the fibroblast cluster in *Atg7^{Δ/Δ}* mice (Fig. 4e). These findings suggest that
281 Cluster 4 may represent cells in the hypothalamus that are negatively impacted by loss of
282 autophagy and that are restored by co-deletion of *Ccl2*.

283

284 Positive logFC values in Cluster 4 had significant upregulation of hypocretin (*Hcrt*), which
285 encodes the neuropeptide orexin, and pro-melanin-concentrating hormone (*Pmch*), the precursor

286 gene that encodes the neuropeptide melanin-concentrating hormone (MCH) (Fig.4f). Both orexin
287 and pro-MCH are orexigenic hormones that stimulate appetite. To validate the snRNA-seq gene
288 expression analysis from Cluster 4, qRT-PCR analysis was used to measure pro-MCH mRNA
289 expression in the hypothalamus. Hypothalami from *Atg7^{Δ/Δ}* mice had decreased mRNA expression,
290 while *Ccl2^{-/-};Atg7^{Δ/Δ}* mice had restored mRNA expression similar to *Atg7^{+/+}* and *Ccl2^{-/-}* mice
291 (Fig. S3d). This data suggested that loss of autophagy leads to CCL2-dependent degradation of
292 cells represented by Cluster 4, which is composed of neurons that produce pro-MCH and orexins,
293 both orexigenic neuropeptides. Thus, the CCL2-induced defective food intake in *Atg7^{Δ/Δ}* mice may
294 be due to degradation of neurons that produce positive regulators of appetite, the loss of which
295 may be lethal (Fig. 4g).

296

297 **Preservation of appetite rescues survival of autophagy-deficient mice**

298 To test the hypothesis that inhibition of food intake was lethal to autophagy-deficient mice we
299 evaluated if eliminating leptin, an appetite suppressing hormone that signals through the
300 hypothalamus, could rescue their defective food intake and survival. Leptin-deficient humans and
301 mice are obese due to their inability to suppress appetite and food intake⁴⁰. Leptin deficient (*ob/ob*)
302 mice⁴¹ were crossed with *Ubc-Cre^{ERT2/+};Atg7^{flox/flox}* mice to generate *ob/ob;Ubc-*
303 *Cre^{ERT2/+};Atg7^{flox/flox}* mice. TAM administration was used to delete *Atg7* in the presence or absence
304 of leptin. Leptin deficiency rescued lethality of autophagy deficient *ob/ob;Atg7^{Δ/Δ}* mice, which
305 survived >250 days post deletion (Fig. 5a). Representative images of each mouse genotype show
306 the weight distribution between respective groups (Fig. 5b). *ob/ob* and *ob/ob;Atg7^{Δ/Δ}* mice had
307 similar obese body weights, and fat mass compared to cachectic *Atg7^{Δ/Δ}* mice (Fig. 5c,d). Lean
308 mass was comparable between *ob/ob;Atg7^{Δ/Δ}* and *Atg7^{Δ/Δ}* mice. (Fig. 5e). Additionally, the levels
309 CCL2 were comparable in *ob/ob;Atg7^{Δ/Δ}* and *Atg7^{Δ/Δ}* mice indicating that leptin deficiency does
310 not rescue survival of autophagy-deficient mice by eliminating CCL2 (Fig. 5f). Leptin deficiency
311 also rescued fasting lethality of autophagy-deficient mice due to the rescue of hypoglycemia and
312 cachexia (Fig. 5g). Lastly, food intake was also rescued in in *ob/ob;Atg7^{Δ/Δ}* and *Atg7^{Δ/Δ}* mice (Fig.
313 5h). Thus, autophagy-deficient mice die due to CCL2-mediated suppression of appetite and food
314 intake that can be rescued by increasing appetite and food intake by deleting leptin (Fig. 5i). As
315 autophagy-deficient mice fail to survive fasting, loss of appetite and food intake is lethal.

316

317 **Discussion**

318 CCL2 is induced in activated microglia in neuroinflammatory diseases and its transgenic
319 expression in mice is sufficient to produce neuronal damage. CCL2 and its receptor CCR2 are
320 associated with STAT2 and IL1 β activation and neurodegeneration^{32,42,43}, but the mechanisms
321 involved are unclear. CCL2 is also associated with cachexia in cancer models. Administration of
322 CCL2 to mice induces wasting of skeletal muscle⁴⁴ and recruitment of macrophages by CCL2 to
323 tumors promotes cachexia⁴⁵, by unknown mechanisms. The lack of food intake in the *Atg7*-
324 deficient mice is associated with anorexia mediated in the hypothalamus. This is distinct from the
325 effect that GDF15 and the inflammatory cytokine IL-6 that seem to mediate anorexia via receptors
326 in the area postrema.

327
328 The chronic loss of the rat MCH-precursor *Pmch* decreases food intake^{46,47} and also affects energy
329 expenditure⁴⁶, thus providing insight into the changed body weight dynamics during chronic loss
330 of *Pmch*. These findings are consistent with loss of autophagy promoting damage,
331 neuroinflammation and CCL2 that destroys MCH-producing orexigenic neurons in the
332 hypothalamus that drive cachexia. Our findings also suggest that targeting CCL2 for degenerative
333 diseases needs to be reexamined due to technical limitations of the approaches in the past.
334 Cachexia is a feature of neurodegenerative and other unresolvable diseases^{48,49}. Our findings
335 provide powerful evidence that CCL2 is a cachexic factor that works by suppressing appetite by
336 inhibiting neurons that produce orexigenic peptides. Clear demonstration that CCL2-induced loss
337 of appetite causes lethal cachexia derived from our ability to restore appetite, prevent weight loss
338 and rescue lethal cachexia by eliminating leptin.

339
340 Autophagy protects from numerous degradative and inflammatory diseases, and this knowledge
341 has provoked efforts to enhance autophagy for therapeutic benefit⁵⁰. Our findings reveal that much
342 of the damage from autophagy inhibition is surprisingly mediated by CCL2. The orexigenic MCH
343 neurons that are the target of CCL2 express a CCL2 receptor, CCR2³⁸, but not CCL2 itself. Thus,
344 loss of autophagy that triggers production of CCL2 occurs in cells other than the HCRT and MCH
345 neurons themselves, perhaps in fibroblasts within the hypothalamus or in activated microglia.
346 These findings also suggest that tissue damage, for example through inhibition of autophagy as
347 shown here, is greatly amplified by the ensuing inflammatory response to that damage. Thus,

348 limiting or resolving the inflammatory response rather than trying to prevent the damage is an
349 alternative approach to mitigate neurodegeneration and other degenerative conditions. Finally, we
350 demonstrate how destructively lethal cachexia can be, as autophagy-deficient mice, despite having
351 several other afflictions, die because they stop eating, illustrating the importance of addressing
352 mechanisms underlying cachexia.

353

354

355

356

357

358

359

360

361

362

363

364

365 **Author contributions**

366 MI designed, performed genomic data analysis. MGJ, A. Sawant, ECL, and ETM assisted with
367 mice experiments. JA-S and SMD produced and generated C1142 antibody. ZH assisted with
368 maintaining mouse colonies, ear tagging and antibody treatments. AD, MS, and SS assisted with
369 genotyping. JDR, XS, TGA, MDG, and TJ provided data analysis, result interpretation, and
370 contributed valuable suggestions. YP, A. Scheinfeld, and ZZ supported the sequencing,
371 interpreted results, and assisted with writing. EW conceived and supervised the study. All authors
372 read, edited, and approved the manuscript.

373

374 **Acknowledgements**

375 This work was supported by the Ludwig Institute for Cancer Research, Ludwig Princeton
376 Branch, Princeton University of EW, and Cancer Grand Challenges CGCSDF-2021\100003
377 (CRUK) and 1OT2CA278609-01 (NCI) to EW, MDG and TJ, and NIH grant R01 CA163591 to
378 EW, JDR, and NIH grant R01 CA243547 to EW, and NIH grant DP2 AI171161 awarded to Y.P.
379 MI was also supported by postdoctoral fellowship COCR23PRF005 from New Jersey
380 Commission on Cancer Research (NJCCR), MG-J was also supported by 1T32CA257957, ECL
381 was supported by R01 CA243547, and A. Sawant was supported by postdoctoral fellowship
382 DFHS10PPC029 from NJCCR. We thank Rutu Patel, Suman Amjad, Angelina Gruszecki, and
383 Ann Hinrichs for their help with genotyping. SMD and JA-S (LAbCore) were funded directly by
384 Ludwig Cancer Research. We acknowledge support from the Rutgers Cancer Institute
385 Metabolomics Shared Resource (NCI-CCSG P30CA072720-6852), the Biospecimen Repository
386 and Histopathology Service Shared Resource (P30CA072720-5919), and the Immune
387 Monitoring and Flow Cytometry Shared Resource, supported, in part, with funding from NCI-
388 CCSG P30CA072720-6852. The schematic representations were created using BioRender.com.
389 The authors also acknowledge the support from all members of the White laboratory.

390

391 **Materials and Methods**

392 **Mouse Models**

393 All animal care was carried out in compliance with Rutgers University Institutional Animal Care
394 and Use Committee guidelines (IACUC). Ubc-Cre^{ERT2/+} mice⁵¹ (The Jackson Laboratory) and
395 Atg7^{flox/flox} mice¹ (provided by Dr. M. Komatsu, Tokyo Metropolitan Institute of Medical

396 Science) were cross-bred to generate the Ubc-Cre^{ERT2/+}; Atg7^{flox/flox} mice as previously described
397 ²To generate Ubc-Cre^{ERT2/+}; Atg7^{flox/flox}; *Ccl2*^{-/-}; *Ccl2*^{-/-} ²³ (The Jackson Laboratory) were cross-
398 bred with our previously created Ubc-Cre^{ERT2/+}; Atg7^{flox/flox} mice. To generate Ubc-Cre^{ERT2/+};
399 Atg7^{flox/flox}; *Cxcl10*^{-/-}; *CXCL10*^{-/-} ²⁷ (The Jackson Laboratory) were cross-bred with our
400 previously created Ubc-Cre^{ERT2/+}; Atg7^{flox/flox} mice. To Ubc-Cre^{ERT2/+}; Atg7^{flox/flox}; *Lep^{ob}/Lep^{ob}*,
401 *Lep^{ob}/Lep^{ob}* ⁵² (The Jackson Laboratory) were cross-bred with our previously created Ubc-Cre
402 ^{ERT2/+}; Atg7^{flox/flox} mice.

403 **Tamoxifen Preparation and Administration**

404 TAM (T5648, Sigma) was suspended at a concentration of 20 mg/ml, in a mixture of 98%
405 sunflower seed oil and 2% ethanol. For TAM delivery, 200 µl per 20 g of body weight (20mg/kg)
406 were injected intraperitoneally into 8 to 10 weeks old mice. Mice were treated once per day for 4
407 days to delete floxed gene systematically². Ubc-Cre^{ERT2/+}; Atg7^{flox/flox}; *Lep^{ob}/Lep^{ob}* were treated
408 twice per week for 2 weeks.

409 **Survival**

410 For mouse Kaplan-Meier survival curve, mice were monitored daily until they reached the
411 endpoint. The criteria for euthanization were a body condition score of 2, body weight loss of
412 >15%, or natural death.

413 **Fasting**

414 Fasting was conducted as previous described².

415 **Metabolic cages**

416 Two indirect calorimetry systems were used, a 12 cage CLAMS apparatus (Columbus
417 Instruments) and 16 cage Promethion Core Mouse Metabolic System (Sable System
418 International). Mice were maintained on a standard chow diet and single housed for 48–72 h
419 prior to experiment start.
420 During the experiment, mice were single housed under a 12-hour light-dark cycle at 21C and 55
421 % humidity for 7 days. The first 24 hours of data collection was removed from analysis due to
422 acclimation period. Oxygen consumption, CO₂ emission, food consumption, movement, running

423 wheel, and energy expenditure were measured every 15 minutes in the CLAMS and 3 minutes in
424 the Promethion.

425 Locomotor activity, both horizontal and vertical, was determined by a X, Y, and Z infrared light
426 beam system. Stationary locomotor activity was defined as continuous infrared light beam breaks
427 of one single light beam and ambulatory movement as continuous breaks of two or more different
428 light beams.

429 Raw data files were collected and processed by the Promethion software package
430 MacroInterpreter 3, which produced standardized output formats for the metabolic variables of
431 interest at each cage. The processed data generated by MacroInterpreter 3 was then analyzed by
432 the CalR: A Web-based Analysis Tool for Indirect Calorimetry Experiments (<https://calrapp.org>)
433 as described previously⁵³.

434 **Body Composition**

435 Body composition analysis (fat and lean mass) was assessed by the EchoMRITM-100H.
436 Unanesthetized mice were placed in a restraint tube that was inserted into the analyzer for
437 approximately 2 min. The mouse was then returned to its home cage.

438 **GDF15 ELISA**

439 GDF15 concentration in the serum was determined using a Mouse & Rat GDF-15 ELISA Kit
440 Quantikine ELISA Kit (R&D Systems; MGD150) according to the manufacturer's instructions.

441 **Cytokine and chemokine assay**

442 Levels of the secreted cytokines and chemokines were determined using the Procarta Plex[®] 36-
443 plex immunoassay (Thermo Fischer Scientific; Cat No: EPX360-26092-901) for mouse serum
444 and liver tissue. Data were collected using a Luminex-200 system and validated using the
445 xPONENT software package. Aliquots of serum and tissue in duplicate were assayed for the
446 secreted molecules as per manufacturer's instructions using Luminex 200 System and analyzed
447 by ProcartaPlex Analyst 1.0 (Luminex Corporation).

448

449 **CCL2 ELISA**

450 CCL2 concentration in the liver tissue supernatants was determined using a Mouse

451 CCL2/JE/MCP-1 Quantikine ELISA Kit (R&D Systems; MJE00B) according to the
452 manufacturer's instructions.

453 **Production of anti-mCCL2 (C1142)**

454 The complete C1142 mAb (CNTO 888 mouse surrogate) sequence was a kind gift from Janssen
455 Research and Development, LLC. Briefly, the DNA sequences encoding the IgG2a/kappa heavy
456 and light chains of C1142, as well as an irrelevant isotype control mAb were synthesized
457 by a commercial vendor (GeneArt, Invitrogen), with codon optimization for efficient expression
458 in CHO cells. The ORFs were then sub-cloned separately into customized pTT-based heavy and
459 light chain episomal expression vectors under the control of cytomegalovirus (CMV) promoters.
460 Heavy and light chain vectors were co-transfected into ExpiCHO-S cells (Cat. A29133; Gibco)
461 according to the manufacturer's instructions and expression allowed to proceed for 5 days.
462 Secreted monoclonal antibodies were purified from clarified expression media using protein A
463 affinity chromatography with MabSelect beads (Cat. GE17-5199-01; Merck), followed by
464 extensive dialysis against phosphate-buffered saline (PBS) using Slide-A-Lyzer G2 dialysis
465 cassettes (Cat. 87731; Life Technologies).

466 **Serum biochemistry analysis**

467 Blood serum samples were analyzed by the Element DC5X™ Veterinary Chemistry Analyzer
468 (Hesk) performed at Rutgers In Vivo Research Services (IVRS) core facility.

469 **Bulk RNA-seq analysis**

470 At 8 weeks post deletion, liver tissue from *Atg7^{+/+}*, *Atg7^{Δ/Δ}*, *Ccl2^{-/-}*, and *Ccl2^{-/-};Atg7^{Δ/Δ}* were
471 dissected and flash frozen in liquid nitrogen. FastQC v0.11.9
472 (<https://www.bioinformatics.babraham.ac.uk/projects/fastqc/>) was used to assess sequencing
473 quality. Reads were first mapped to the mouse genome using HiSat2 v2.2.1⁵⁴. The genomic
474 index along with the list of splice sites and exons were created by HiSat2 using the genome
475 assembly mm10 from ENSEMBL together with the comprehensive gene annotation from mm10
476 vM23 from Gencode⁵⁵. Gene level counts were computed using Rsubread v2.8.2⁵⁶ (options
477 `isPairedEnd = TRUE`, `requireBothEndsMapped = TRUE`, `minOverlap = 80`,
478 `countChimericFragments = FALSE`).

479 The liver tissue was analyzed separately, and genes were filtered out from further analysis if the
480 mean read count across all samples in the tissue was less than 50. This resulted in 10,563,
481 10,285, and 21,823 genes that went into further analysis of the brown adipose tissue, GNP, and
482 liver data, respectively. DESeq2 v1.34.0⁵⁷ was used to perform differential gene expression
483 analysis. Differentially expressed genes were used for further analysis and visualization. Gene
484 expression heatmaps were generated with pheatmap v1.0.12 ([https://cran.r-](https://cran.r-project.org/web/packages/pheatmap/index.html)
485 [project.org/web/packages/pheatmap/index.html](https://cran.r-project.org/web/packages/pheatmap/index.html)) using values that were z-score normalized for
486 each gene across all samples within each tissue. Volcano plots were generated with
487 EnhancedVolcano v1.12.0 (<https://github.com/kevinblighe/EnhancedVolcano>). All analysis
488 starting from count table generation was conducted in the R statistical environment v4.1.3.

489 **snRNA-seq analysis:**

490 At 8 weeks post deletion, hypothalamus tissue from *Atg7^{+/+}*, *Atg7^{Δ/Δ}*, *Ccl2^{-/-}*, and
491 *Ccl2^{-/-};Atg7^{Δ/Δ}* were dissected and flash frozen in liquid nitrogen. Downstream analysis was
492 carried out using the scanpy package v1.9.3⁵⁸. Initial quality control steps and normalization
493 were carried out separately for each of the four samples. Cells were filtered out if they had high
494 relative mitochondrial UMI counts (>4-10% for *Atg7^{+/+}*, *Atg7^{Δ/Δ}*, *Ccl2^{-/-}*, and *Ccl2^{-/-};Atg7^{Δ/Δ}*)
495 and high total counts (>15,000-20,000 for *Atg7^{+/+}*, *Atg7^{Δ/Δ}*, *Ccl2^{-/-}*, and *Ccl2^{-/-};Atg7^{Δ/Δ}*), which
496 resulted in the removal of 150-300 cells for *Atg7^{+/+}*, *Atg7^{Δ/Δ}*, *Ccl2^{-/-}*, and *Ccl2^{-/-};Atg7^{Δ/Δ}*. Cells
497 with the potential of being doublets (score >0.2 as detected by Scrublet, 200-250 cells in each
498 sample, respectively) were also removed. Genes were filtered out from the subsequent analysis if
499 they were present in <1% of cells in the sample. Gene expression counts were then normalized
500 with analytical Pearson residual normalization from scanpy, using a theta value of 10 for all four
501 of the samples. After normalization, the four samples were concatenated. Non-protein-coding
502 genes (2,447 genes, 1.6% of total UMI counts) were also filtered out on the basis of the
503 CellRanger mm10 GTF file vM23. This resulted in a dataset of 20,297 cells and 1,600 genes.

504 PCA was run with 100 components, a kNN graph was built using 30 neighbors, 70 PCs and
505 cosine metric, and Leiden clustering was carried out with a resolution of 2.1, resulting in 52
506 clusters. Known marker genes from HypoMap⁵⁸ were used to annotate the Leiden clusters using
507 the score genes function in scanpy and by exploring differentially expressed genes in each cluster
508 as compared with all cells outside the cluster, obtained using a custom script. For differential

509 expression analysis, log₂ fold change (log₂FC) of expression was calculated as the ratio of
510 pseudobulk raw UMI counts summed over cells within and outside the cluster (then normalized
511 by total amount of UMI counts inside and outside the cluster), p-values were calculated using
512 Mann-Whitney U test applied to Pearson residual normalized expression values in single cells
513 within and outside the cluster, and Bonferroni correction for multiple hypothesis testing applied
514 to all genes with $\text{abs}(\log_2\text{FC}) > 0.5$.

515 **Tolerance Test**

516 LL-lactate tolerance tests were performed after 6 h of fasting. Mice were injected
517 intraperitoneally with L-lactate (2 g/kg BW). Blood glucose levels (Accu-Chek Performa
518 glucometer) were determined from the tail vein at 0, 15, 30, 45, 60, and 120 min after injection
519 (Accu-Chek Performa glucometer).

520 **Histologic and immunohistochemical analysis**

521 Mouse tissues were collected and fixed in 10% formalin solution (Formaldehyde Fresh, Fisher
522 Scientific, SF94-4). Tissues were fixed overnight and then transferred to 70% ethanol for
523 paraffin-embedded sections. The slides were deparaffinized, rehydrated and hematoxylin–eosin
524 staining was performed.

525 **Metabolite analysis by LC–MS**

526 Metabolites were extracted as described previously⁵⁹. Briefly, metabolites were extracted from
527 serum using the extraction buffer containing methanol: acetonitrile: H₂O (40:40:20). The final
528 extract was stored at –80 °C until analysis by LC–MS. The LC-MS metabolomic analysis was
529 performed at the Metabolomics Shared Resource of Rutgers Cancer Institute on a Q Exactive
530 PLUS hybrid quadrupole-orbitrap mass spectrometer coupled to a Vanquish Horizon UHPLC
531 system (Thermo Fisher Scientific, Waltham, MA) with an XBridge BEH Amide column (150
532 mm × 2.1 mm, 2.5 μm particle size, Waters, Milford, MA). The HILIC separation used a
533 gradient of solvent A (95%:5% H₂O:acetonitrile with 20 mM acetic acid, 40 mM ammonium
534 hydroxide, pH 9.4) and solvent B (20%:80% H₂O:acetonitrile with 20 mM acetic acid, 40 mM
535 ammonium hydroxide, pH 9.4). The gradient was 0 min, 100% B; 3 min, 100% B; 3.2 min, 90%
536 B; 6.2 min, 90% B; 6.5 min, 80% B; 10.5 min, 80% B; 10.7 min, 70% B; 13.5 min, 70% B; 13.7
537 min, 45% B; 16 min, 45% B; 16.5 min, 100% B; and 22 min, 100% B⁶⁰. The flow rate was 300

538 $\mu\text{L}/\text{min}$. The column temperature was set to $25\text{ }^\circ\text{C}$. The autosampler temperature was set to $4\text{ }^\circ\text{C}$,
539 and the injection volume was $5\text{ }\mu\text{L}$. MS scans were obtained in negative ionization mode with a
540 resolution of 70,000 at m/z 200, in addition to an automatic gain control target of 3×10^6 and m/z
541 scan range of 72 to 1000. Metabolite data was obtained using the MAVEN software package⁶¹
542 (mass accuracy window: 5 ppm).

543 **Labelled Lactate infusion**

544 For intra-jugular vein catheterization, the procedure was performed as described previously⁵⁹.
545 Briefly, venous catheters were surgically implanted into the jugular veins of *Atg7 Δ/Δ* , *Atg7 $^{+/+}$* ,
546 *Ccl2 $^{-/-}$* , *Ccl2 $^{-/-}; Atg7 $\Delta/\Delta$$* mice at 5 weeks post TAM injection. On the day of infusion, mice were
547 fasted for 6 hours. Mice were infused with ^{13}C -Lactate (CLM-1579-PK) dissolved in sterile
548 saline at a rate of $0.1\text{ }\mu\text{L}/\text{g}/\text{min}$ for 2.5 hours. Mice were sacrificed after infusion for serum
549 analysis by LC-MS.

550 **Real-time PCR**

551 Total RNA was isolated from hypothalami by Qiagen RNA micro kit (Qiagen). cDNA was then
552 reverse transcribed from the total RNA by MultiScribe RT kit (Thermo Scientific). Real-time
553 PCR were performed on Applied Biosystems StepOne Plus machine using SYBR green master
554 mix (Thermo Scientific). Results were calculated using $\Delta\Delta\text{Ct}$ method and then normalized to
555 actin.

556 **Statistical analysis**

557 Statistical analysis was performed with GraphPad Prism (V.6). A Student's t-test or a one-way
558 analysis of variance (ANOVA) was used for comparison between the groups. A two-way
559 ANOVA was used for repeated measures for comparisons between the groups. A post-hoc
560 comparison using Tukey HSD was applied according to the two-way ANOVA results. Statistical
561 significance was set at $p < 0.05$.

562

563

564

565
566
567
568
569
570
571
572
573
574
575
576
577
578
579
580
581
582
583
584
585
586
587
588
589
590
591
592
593
594
595
596
597
598
599
600
601
602
603
604
605
606
607
608
609

References

- 1 Komatsu, M. *et al.* Impairment of starvation-induced and constitutive autophagy in Atg7-deficient mice. *J Cell Biol* **169**, 425-434 (2005). <https://doi.org/10.1083/jcb.200412022>
- 2 Karsli-Uzunbas, G. *et al.* Autophagy is required for glucose homeostasis and lung tumor maintenance. *Cancer Discov* **4**, 914-927 (2014). <https://doi.org/10.1158/2159-8290.CD-14-0363>
- 3 Yang, Y. *et al.* Autophagy promotes mammalian survival by suppressing oxidative stress and p53. *Genes Dev* **34**, 688-700 (2020). <https://doi.org/10.1101/gad.335570.119>
- 4 Rabinowitz, J. D. & White, E. Autophagy and metabolism. *Science* **330**, 1344-1348 (2010). <https://doi.org/10.1126/science.1193497>
- 5 Mizushima, N. & Komatsu, M. Autophagy: renovation of cells and tissues. *Cell* **147**, 728-741 (2011). <https://doi.org/10.1016/j.cell.2011.10.026>
- 6 Mizushima, N. & Kuma, A. Autophagosomes in GFP-LC3 Transgenic Mice. *Methods Mol Biol* **445**, 119-124 (2008). https://doi.org/10.1007/978-1-59745-157-4_7
- 7 Kuma, A. *et al.* The role of autophagy during the early neonatal starvation period. *Nature* **432**, 1032-1036 (2004). <https://doi.org/10.1038/nature03029>
- 8 Yang, Y. *et al.* Autophagy in PDGFRalpha+ mesenchymal cells is essential for intestinal stem cell survival. *Proc Natl Acad Sci U S A* **119**, e2202016119 (2022). <https://doi.org/10.1073/pnas.2202016119>
- 9 Yoshii, S. R. *et al.* Systemic Analysis of Atg5-Null Mice Rescued from Neonatal Lethality by Transgenic ATG5 Expression in Neurons. *Dev Cell* **39**, 116-130 (2016). <https://doi.org/10.1016/j.devcel.2016.09.001>
- 10 Poillet-Perez, L. *et al.* Autophagy promotes growth of tumors with high mutational burden by inhibiting a T-cell immune response. *Nat Cancer* **1**, 923-934 (2020). <https://doi.org/10.1038/s43018-020-00110-7>
- 11 Poillet-Perez, L. *et al.* Autophagy maintains tumour growth through circulating arginine. *Nature* **563**, 569-573 (2018). <https://doi.org/10.1038/s41586-018-0697-7>
- 12 Ueno, T. & Komatsu, M. Autophagy in the liver: functions in health and disease. *Nat Rev Gastroenterol Hepatol* **14**, 170-184 (2017). <https://doi.org/10.1038/nrgastro.2016.185>
- 13 Komatsu, M. *et al.* Loss of autophagy in the central nervous system causes neurodegeneration in mice. *Nature* **441**, 880-884 (2006). <https://doi.org/10.1038/nature04723>
- 14 Hara, T. *et al.* Suppression of basal autophagy in neural cells causes neurodegenerative disease in mice. *Nature* **441**, 885-889 (2006). <https://doi.org/10.1038/nature04724>
- 15 Guo, F., Liu, X., Cai, H. & Le, W. Autophagy in neurodegenerative diseases: pathogenesis and therapy. *Brain Pathol* **28**, 3-13 (2018). <https://doi.org/10.1111/bpa.12545>
- 16 Singh, R. *et al.* Autophagy regulates lipid metabolism. *Nature* **458**, 1131-1135 (2009). <https://doi.org/10.1038/nature07976>
- 17 Yule, M. S., Brown, L. R., Skipworth, R. J. E. & Laird, B. J. A. Central neural mechanisms of cancer cachexia. *Curr Opin Support Palliat Care* **18**, 138-144 (2024). <https://doi.org/10.1097/SPC.0000000000000707>
- 18 Olson, B., Diba, P., Korzun, T. & Marks, D. L. Neural Mechanisms of Cancer Cachexia. *Cancers (Basel)* **13** (2021). <https://doi.org/10.3390/cancers13163990>

- 610 19 Cimino, I., Coll, A. P. & Yeo, G. S. H. GDF15 and energy balance: homing in on a
611 mechanism. *Nat Med* **23**, 1119-1120 (2017). <https://doi.org/10.1038/nm.4414>
- 612 20 Hsu, J. Y. *et al.* Non-homeostatic body weight regulation through a brainstem-restricted
613 receptor for GDF15. *Nature* **550**, 255-259 (2017). <https://doi.org/10.1038/nature24042>
- 614 21 Mullican, S. E. *et al.* GFRAL is the receptor for GDF15 and the ligand promotes weight
615 loss in mice and nonhuman primates. *Nat Med* **23**, 1150-1157 (2017).
616 <https://doi.org/10.1038/nm.4392>
- 617 22 Emmerson, P. J. *et al.* The metabolic effects of GDF15 are mediated by the orphan
618 receptor GFRAL. *Nat Med* **23**, 1215-1219 (2017). <https://doi.org/10.1038/nm.4393>
- 619 23 Lu, B. *et al.* Abnormalities in monocyte recruitment and cytokine expression in monocyte
620 chemoattractant protein 1-deficient mice. *J Exp Med* **187**, 601-608 (1998).
621 <https://doi.org/10.1084/jem.187.4.601>
- 622 24 Wang, D. *et al.* GDF15 promotes weight loss by enhancing energy expenditure in muscle.
623 *Nature* **619**, 143-150 (2023). <https://doi.org/10.1038/s41586-023-06249-4>
- 624 25 Zhang, X. *et al.* CXCL10 plays a key role as an inflammatory mediator and a non-
625 invasive biomarker of non-alcoholic steatohepatitis. *J Hepatol* **61**, 1365-1375 (2014).
626 <https://doi.org/10.1016/j.jhep.2014.07.006>
- 627 26 Tomita, K. *et al.* CXCL10-Mediates Macrophage, but not Other Innate Immune Cells-
628 Associated Inflammation in Murine Nonalcoholic Steatohepatitis. *Sci Rep* **6**, 28786
629 (2016). <https://doi.org/10.1038/srep28786>
- 630 27 Dufour, J. H. *et al.* IFN-gamma-inducible protein 10 (IP-10; CXCL10)-deficient mice
631 reveal a role for IP-10 in effector T cell generation and trafficking. *J Immunol* **168**, 3195-
632 3204 (2002). <https://doi.org/10.4049/jimmunol.168.7.3195>
- 633 28 Roca, H. *et al.* CCL2 and interleukin-6 promote survival of human CD11b+ peripheral
634 blood mononuclear cells and induce M2-type macrophage polarization. *J Biol Chem* **284**,
635 34342-34354 (2009). <https://doi.org/10.1074/jbc.M109.042671>
- 636 29 Luciano-Mateo, F. *et al.* Chemokine C-C motif ligand 2 overexpression drives tissue-
637 specific metabolic responses in the liver and muscle of mice. *Sci Rep* **10**, 11954 (2020).
638 <https://doi.org/10.1038/s41598-020-68769-7>
- 639 30 Sell, H., Dietze-Schroeder, D., Kaiser, U. & Eckel, J. Monocyte chemotactic protein-1 is
640 a potential player in the negative cross-talk between adipose tissue and skeletal muscle.
641 *Endocrinology* **147**, 2458-2467 (2006). <https://doi.org/10.1210/en.2005-0969>
- 642 31 Sasaki, Y. *et al.* NOX4 Regulates CCR2 and CCL2 mRNA Stability in Alcoholic Liver
643 Disease. *Sci Rep* **7**, 46144 (2017). <https://doi.org/10.1038/srep46144>
- 644 32 Bose, S. & Cho, J. Role of chemokine CCL2 and its receptor CCR2 in neurodegenerative
645 diseases. *Arch Pharm Res* **36**, 1039-1050 (2013). <https://doi.org/10.1007/s12272-013-0161-z>
- 646
- 647 33 Haringman, J. J. *et al.* A randomized controlled trial with an anti-CCL2 (anti-monocyte
648 chemotactic protein 1) monoclonal antibody in patients with rheumatoid arthritis.
649 *Arthritis Rheum* **54**, 2387-2392 (2006). <https://doi.org/10.1002/art.21975>
- 650 34 Tsui, P. *et al.* Generation, characterization and biological activity of CCL2 (MCP-1/JE)
651 and CCL12 (MCP-5) specific antibodies. *Hum Antibodies* **16**, 117-125 (2007).
- 652 35 Loberg, R. D. *et al.* Targeting CCL2 with systemic delivery of neutralizing antibodies
653 induces prostate cancer tumor regression in vivo. *Cancer Res* **67**, 9417-9424 (2007).
654 <https://doi.org/10.1158/0008-5472.CAN-07-1286>

- 655 36 Pienta, K. J. *et al.* Phase 2 study of carlumab (CNTO 888), a human monoclonal antibody
656 against CC-chemokine ligand 2 (CCL2), in metastatic castration-resistant prostate cancer.
657 *Invest New Drugs* **31**, 760-768 (2013). <https://doi.org/10.1007/s10637-012-9869-8>
- 658 37 Fleming, A. *et al.* The different autophagy degradation pathways and neurodegeneration.
659 *Neuron* **110**, 935-966 (2022). <https://doi.org/10.1016/j.neuron.2022.01.017>
- 660 38 Le Thuc, O. *et al.* Central CCL2 signaling onto MCH neurons mediates metabolic and
661 behavioral adaptation to inflammation. *EMBO Rep* **17**, 1738-1752 (2016).
662 <https://doi.org/10.15252/embr.201541499>
- 663 39 Steuernagel, L. *et al.* HypoMap-a unified single-cell gene expression atlas of the murine
664 hypothalamus. *Nat Metab* **4**, 1402-1419 (2022). [https://doi.org/10.1038/s42255-022-](https://doi.org/10.1038/s42255-022-00657-y)
665 [00657-y](https://doi.org/10.1038/s42255-022-00657-y)
- 666 40 Ewart-Toland, A., Mounzih, K., Qiu, J. & Chehab, F. F. Effect of the genetic background
667 on the reproduction of leptin-deficient obese mice. *Endocrinology* **140**, 732-738 (1999).
668 <https://doi.org/10.1210/endo.140.2.6470>
- 669 41 Fantuzzi, G. & Faggioni, R. Leptin in the regulation of immunity, inflammation, and
670 hematopoiesis. *J Leukoc Biol* **68**, 437-446 (2000).
- 671 42 Tian, D. S. *et al.* Chemokine CCL2-CCR2 Signaling Induces Neuronal Cell Death via
672 STAT3 Activation and IL-1beta Production after Status Epilepticus. *J Neurosci* **37**, 7878-
673 7892 (2017). <https://doi.org/10.1523/JNEUROSCI.0315-17.2017>
- 674 43 Joly-Amado, A. *et al.* CCL2 Overexpression in the Brain Promotes Glial Activation and
675 Accelerates Tau Pathology in a Mouse Model of Tauopathy. *Front Immunol* **11**, 997
676 (2020). <https://doi.org/10.3389/fimmu.2020.00997>
- 677 44 Alissa, N. *et al.* CCL2 signaling promotes skeletal muscle wasting in non-tumor and
678 breast tumor models. *Dis Model Mech* **17** (2024). <https://doi.org/10.1242/dmm.050398>
- 679 45 Liu, M. *et al.* The crosstalk between macrophages and cancer cells potentiates pancreatic
680 cancer cachexia. *Cancer Cell* **42**, 885-903 e884 (2024).
681 <https://doi.org/10.1016/j.ccell.2024.03.009>
- 682 46 Mul, J. D. *et al.* Chronic loss of melanin-concentrating hormone affects motivational
683 aspects of feeding in the rat. *PLoS One* **6**, e19600 (2011).
684 <https://doi.org/10.1371/journal.pone.0019600>
- 685 47 Mul, J. D. *et al.* Pmch expression during early development is critical for normal energy
686 homeostasis. *Am J Physiol Endocrinol Metab* **298**, E477-488 (2010).
687 <https://doi.org/10.1152/ajpendo.00154.2009>
- 688 48 Ferrer, M. *et al.* Cachexia: A systemic consequence of progressive, unresolved disease.
689 *Cell* **186**, 1824-1845 (2023). <https://doi.org/10.1016/j.cell.2023.03.028>
- 690 49 Plata-Salaman, C. R. Central nervous system mechanisms contributing to the cachexia-
691 anorexia syndrome. *Nutrition* **16**, 1009-1012 (2000). [https://doi.org/10.1016/s0899-](https://doi.org/10.1016/s0899-9007(00)00413-5)
692 [9007\(00\)00413-5](https://doi.org/10.1016/s0899-9007(00)00413-5)
- 693 50 Ichimiya, T. *et al.* Autophagy and Autophagy-Related Diseases: A Review. *Int J Mol Sci*
694 **21** (2020). <https://doi.org/10.3390/ijms21238974>
- 695 51 Ruzankina, Y. *et al.* Deletion of the developmentally essential gene ATR in adult mice
696 leads to age-related phenotypes and stem cell loss. *Cell Stem Cell* **1**, 113-126 (2007).
697 <https://doi.org/10.1016/j.stem.2007.03.002>
- 698 52 Ingalls, A. M., Dickie, M. M. & Snell, G. D. Obese, a new mutation in the house mouse.
699 *Obes Res* **4**, 101 (1996). <https://doi.org/10.1002/j.1550-8528.1996.tb00519.x>

- 700 53 Mina, A. I. *et al.* CalR: A Web-Based Analysis Tool for Indirect Calorimetry
701 Experiments. *Cell Metab* **28**, 656-666 e651 (2018).
702 <https://doi.org/10.1016/j.cmet.2018.06.019>
- 703 54 Kim, D., Langmead, B. & Salzberg, S. L. HISAT: a fast spliced aligner with low memory
704 requirements. *Nat Methods* **12**, 357-360 (2015). <https://doi.org/10.1038/nmeth.3317>
- 705 55 Mudge, J. M. & Harrow, J. Creating reference gene annotation for the mouse C57BL6/J
706 genome assembly. *Mamm Genome* **26**, 366-378 (2015). <https://doi.org/10.1007/s00335-015-9583-x>
- 707
- 708 56 Liao, Y., Smyth, G. K. & Shi, W. The Subread aligner: fast, accurate and scalable read
709 mapping by seed-and-vote. *Nucleic Acids Res* **41**, e108 (2013).
710 <https://doi.org/10.1093/nar/gkt214>
- 711 57 Love, M. I., Huber, W. & Anders, S. Moderated estimation of fold change and dispersion
712 for RNA-seq data with DESeq2. *Genome Biol* **15**, 550 (2014).
713 <https://doi.org/10.1186/s13059-014-0550-8>
- 714 58 Wolf, F. A., Angerer, P. & Theis, F. J. SCANPY: large-scale single-cell gene expression
715 data analysis. *Genome Biol* **19**, 15 (2018). <https://doi.org/10.1186/s13059-017-1382-0>
- 716 59 Khayati, K. *et al.* Autophagy compensates for Lkb1 loss to maintain adult mice
717 homeostasis and survival. *Elife* **9** (2020). <https://doi.org/10.7554/eLife.62377>
- 718 60 Su, X. *et al.* In-Source CID Ramping and Covariant Ion Analysis of Hydrophilic
719 Interaction Chromatography Metabolomics. *Anal Chem* **92**, 4829-4837 (2020).
720 <https://doi.org/10.1021/acs.analchem.9b04181>
- 721 61 Melamud, E., Vastag, L. & Rabinowitz, J. D. Metabolomic analysis and visualization
722 engine for LC-MS data. *Anal Chem* **82**, 9818-9826 (2010).
723 <https://doi.org/10.1021/ac1021166>
- 724

725

726 **Figure 1: Systemic metabolic impairment due to loss of autophagy causes cachexia**

727 **a**, Mouse body mass post TAM injection in *Atg7^{+/+}* mice ($n = 5$) and *Atg7^{Δ/Δ}* mice ($n = 7$) **b,c** Lean
728 mass in grams and fat mass percentage loss post TAM injection in *Atg7^{+/+}* mice ($n = 5$) and *Atg7^{Δ/Δ}*
729 mice ($n = 5$). Body composition was measured by EchoMRI. All data are mean \pm s.e.m. * $P < 0.05$,
730 ** $P < 0.01$, *** $P < 0.01$, **** $P < 0.0001$ using a two-sided Student's *t*-test. **d**, Body mass
731 subtracted by liver weight at 10 weeks post TAM in *Atg7^{+/+}* mice ($n = 4$) and *Atg7^{Δ/Δ}* mice ($n = 5$)
732 **e–j**, Mice were housed in Promethion metabolic cages ($n = 4–21$ /group). Shaded regions represent
733 the dark cycle from 19:00 pm to 7:00 am. **e**, daily ambulatory activity at 2- and 8- weeks post TAM
734 . **f**, total wheel running at 2 weeks post TAM. **g**, Hourly mean of RER at 2- and 8- weeks post
735 TAM. **h**, Overall hourly means of RER at 2- and 8- weeks post TAM. **i**, Total energy expenditure.
736 **j**, daily food intake. **k**, Serum (GDF15 ELISA) and cytokine and chemokine profiling (CXCL10
737 and CCL2) ($n = 5–11$ /group) of *Atg7^{+/+}* and *Atg7^{Δ/Δ}* mice.

738

739 **Figure 2: Induction of CCL2 contributes to lethality during autophagy deficiency**

740 **a**, Kaplan-Meier survival curve of *Atg7^{+/+}*, *Atg7^{Δ/Δ}*, *Ccl2^{-/-}*, and *Ccl2^{-/-};Atg7^{Δ/Δ}* mice. **b**,
741 Representative images of *Atg7^{+/+}*, *Atg7^{Δ/Δ}*, *Ccl2^{-/-}*, and *Ccl2^{-/-};Atg7^{Δ/Δ}* mice at 8- and 42- weeks
742 post TAM injection. **c**, Kaplan-Meier 24 hours fasting survival curve of *Atg7^{+/+}*, *Atg7^{Δ/Δ}*, *Ccl2^{-/-}*,
743 and *Ccl2^{-/-};Atg7^{Δ/Δ}* mice 10 days post-TAM. **d**, Blood glucose and plasma insulin measurements
744 collected at 16-hour post fast. **e**, Blood glucose following an intraperitoneal lactate tolerance
745 test. Area under curve calculated from individual blood glucose traces. (*) $P < 0.05$; (***) $P <$
746 0.001 ; (****) $P < 0.0001$; (n.s.) not significant (unpaired *t*-test). **f–i**, Statistical analysis of the
747 main altered metabolites enrichment in plasma of *Atg7^{+/+}*, *Atg7^{Δ/Δ}*, *Ccl2^{-/-}*,
748 and *Ccl2^{-/-};Atg7^{Δ/Δ}* mice after *in vivo* ¹³C lactate tracing at 2 weeks post deletion. **f**, Lactate
749 enrichment **h**, glucose enrichment **i**, ratio glucose/lactate enrichment. For all graphs the *P* values
750 were determined using one-way ANOVA. *P* values are indicated as $\leq 0.05^*$, $\leq 0.01^{**}$, $\leq 0.001^{***}$,
751 and $\leq 0.0001^{****}$.

752

753 **Figure 3: Metabolic Phenotyping shows Loss of CCL2 impacts body composition and food**
754 **intake.**

755 **a**, Mouse body weight post TAM injection in *Atg7^{+/+}*, *Atg7^{Δ/Δ}* mice, *Ccl2^{-/-}* mice,
756 and *Ccl2^{-/-};Atg7^{Δ/Δ}* mice over 365 days. **b,c** Lean mass and fat mass over 42 weeks post TAM
757 injection in *Atg7^{+/+}*, *Atg7^{Δ/Δ}* mice, *Ccl2^{-/-}* mice, and *Ccl2^{-/-};Atg7^{Δ/Δ}*. Body composition was
758 measured by EchoMRI. All data are mean \pm s.e.m. * $P < 0.05$, ** $P < 0.01$, *** $P < 0.01$,
759 **** $P < 0.0001$ using a two-sided Student's *t*-test. **d–h**, Mice were housed in Promethion
760 metabolic cages ($n = 4–11$ /group). Shaded regions represent the dark cycle from 19:00 pm to 7:00
761 am. **d**, daily ambulatory activity at 2 weeks post TAM. **e**, Hourly mean of RER at 2- and 8- weeks
762 post TAM. **f**, Overall hourly means of RER at 2- and 8- weeks post TAM. **g**, Total energy
763 expenditure. **h**, daily food intake.

764

765 **Figure 4: Diversity and proportion of cell types in the scRNA-seq of the hypothalamus from**
766 **wild-type and *Ccl2^{-/-}* mice with and without deletion of *Atg7*.**

767 **a**, Uniform Manifold Approximation and Projection (UMAP) of the snRNA-seq data with cell
768 type annotations for *Atg7^{Δ/Δ}*, *Ccl2^{-/-}*, and *Ccl2^{-/-};Atg7^{Δ/Δ}* mice at the 8-wk time point. **b**, UMAP
769 showing 52 clusters that were used to annotate cell types. **c**, UMAP showing the cells separately
770 for *Atg7^{Δ/Δ}*, *Ccl2^{-/-}*, and *Ccl2^{-/-};Atg7^{Δ/Δ}* mice. **d**, Bar plot depicting the cluster composition across

771 the different samples. **e**, Expression of CCL2 across cell types in *Atg7^{Δ/Δ}* mice. **f**, Top 10
772 upregulated genes in Cluster 4. **g**, Schematic of snRNA-seq results due to loss of CCL2.

773

774 **Figure 5: *ob/ob* rescues lethality and weight loss induced by autophagy deficiency.**

775 **a**, Kaplan-Meier survival curve of *Atg7^{+/+}*, *Atg7^{Δ/Δ}*, *ob/ob*, and *ob/ob;Atg7^{Δ/Δ}* mice. **b**,

776 Representative images of *Atg7^{+/+}*, *Atg7^{Δ/Δ}* mice, *ob/ob* mice, and *ob/ob;Atg7^{Δ/Δ}* mice at 8- and 42-

777 weeks post TAM injection. **c**, Mouse body weight post TAM injection in

778 *Atg7^{+/+}*, *Atg7^{Δ/Δ}* mice, *ob/ob* mice, and *ob/ob;Atg7^{Δ/Δ}* mice. **d-e**, Fat mass and lean mass loss post

779 TAM injection in mice. Body composition was measured by EchoMRI. All data are mean ± s.e.m.

780 **P* < 0.05, ***P* < 0.01, ****P* < 0.01, *****P* < 0.0001 using a two-sided Student's *t*-test. **f**, Serum

781 CCL2 ELISA. **g**, Kaplan-Meier 24 hours fasting survival curve of *Atg7^{+/+}*, *Atg7^{Δ/Δ}*, *ob/ob*,

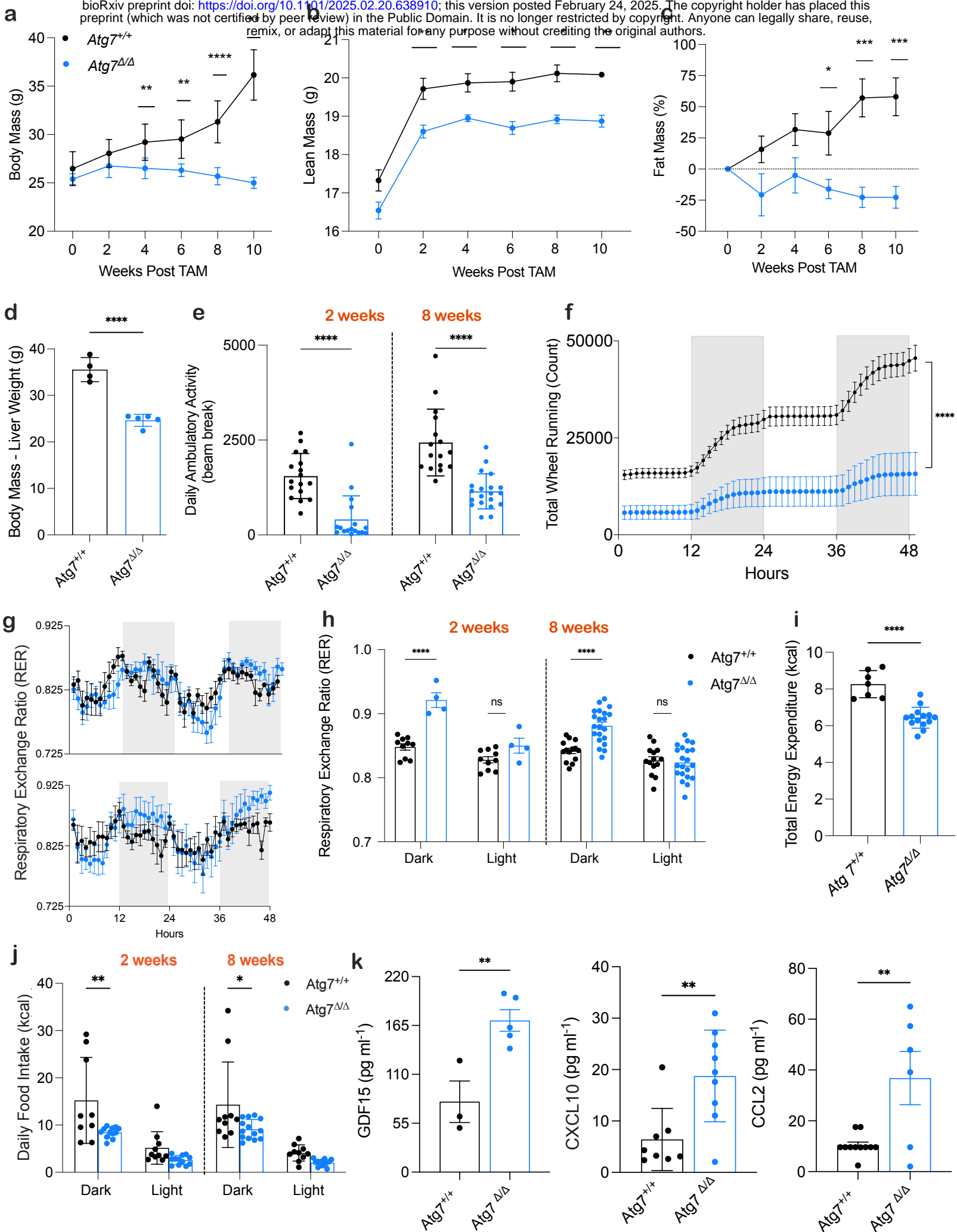
782 and *ob/ob;Atg7^{Δ/Δ}* mice 10 days post-TAM. Blood glucose collected at 16-hour post fast. **h**, daily

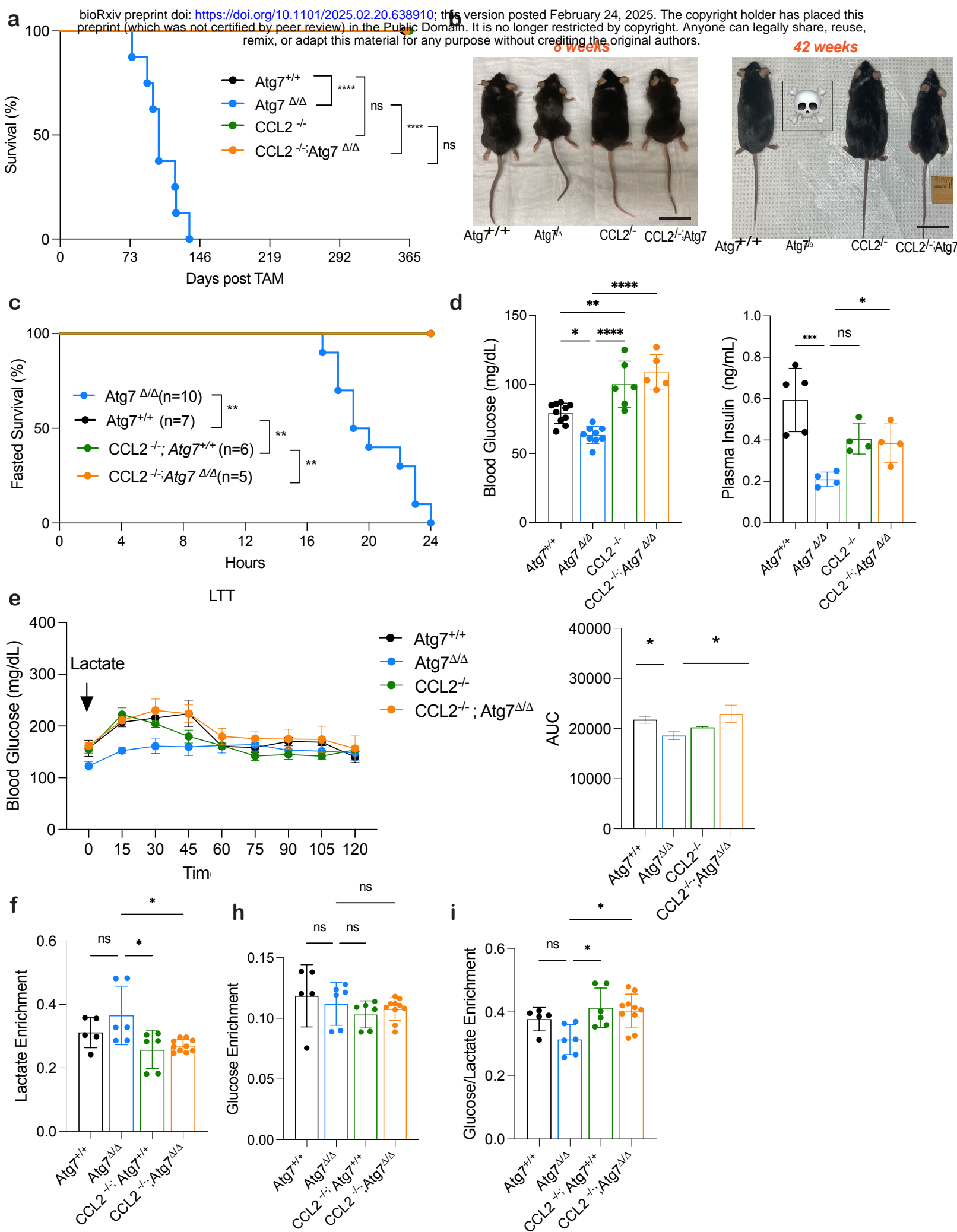
783 food intake. **k**, Proposed graphical summary of lethality in autophagy deficient mice.

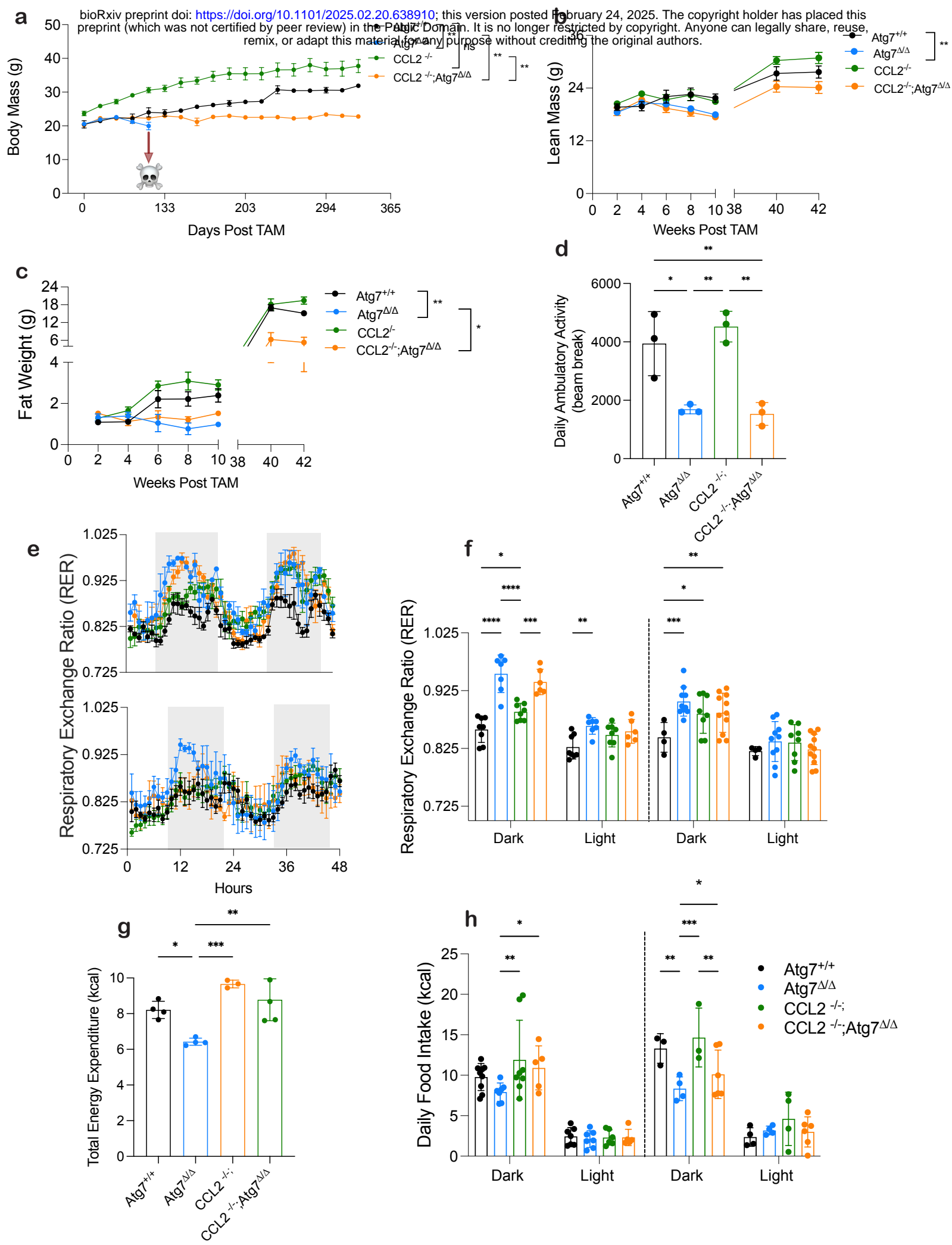
784

785

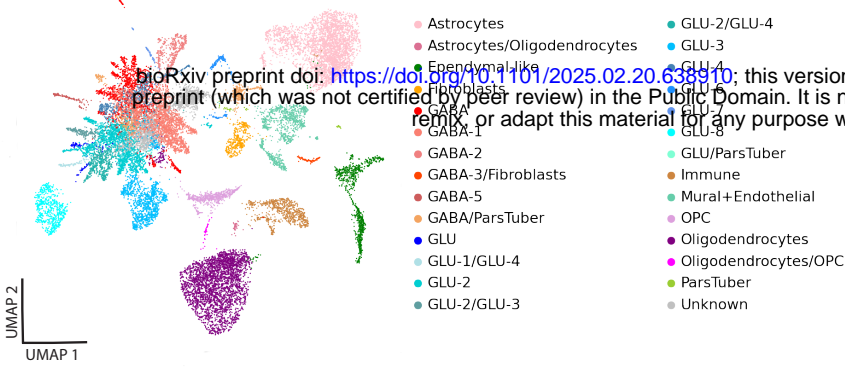
786



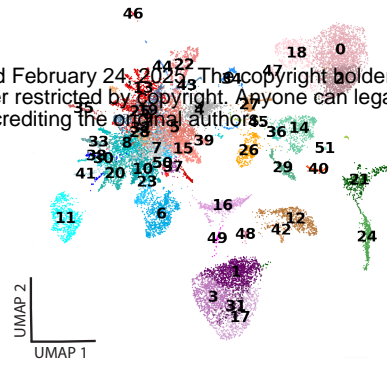




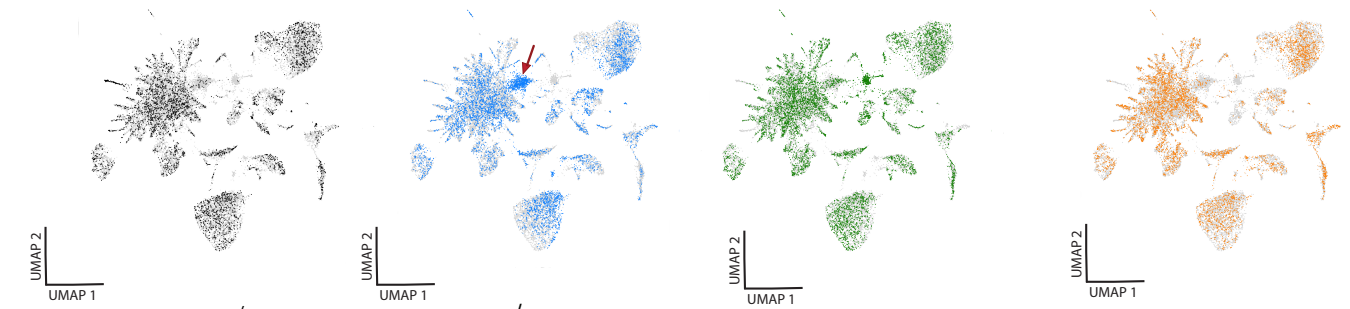
a



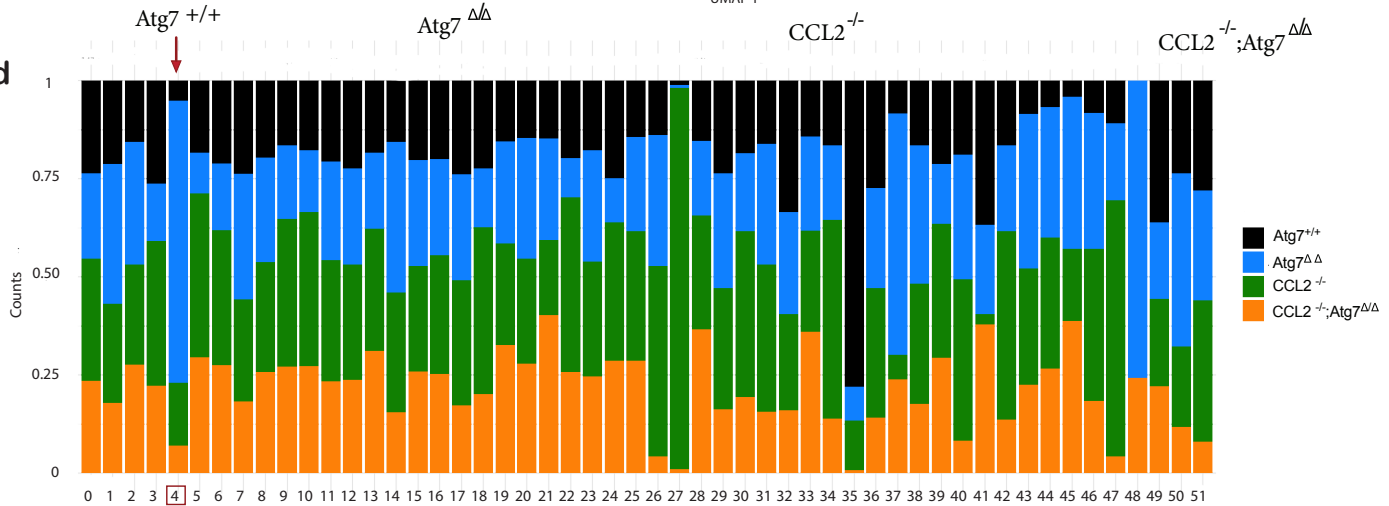
b



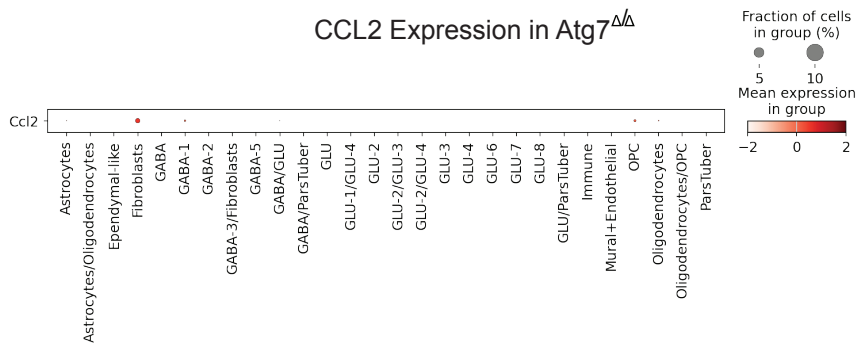
c



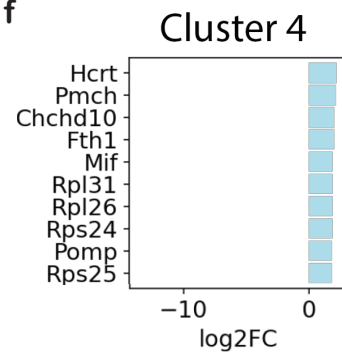
d



e



f



g

